Journal Name

RSCPublishing

ARTICLE

Anionic coordination complexes of C_{60} and C_{70} with cyclopentadienyl and pentamethylcyclopentadienyl molybdenum dicarbonyl

Cite this: DOI: 10.1039/x0xx00000x

Received 00th January 2012,
Accepted 00th January 2012

DOI: 10.1039/x0xx00000x

www.rsc.org/

Dmitri V. Konarev,*[a] Alexey V. Kuzmin,[b] Sergey I. Troyanov,[c] Yoshiaki Nakano,[d] Salavat S. Khasanov,[b] Akihiro Otsuka,[d] Hideki Yamochi,[d] Gunzi Saito,[e] and Rimma N. Lyubovskaya[a]

Crystalline anionic coordination complexes $(PPN^+)\{CpMo(CO)_2(\eta^2\text{-}C_{60})\}^-$ (**1**), $(PPN^+)\{CpMo(CO)_2(\eta^2\text{-}C_{70})\}^-$ (**2**) and $(PPN^+)\{Cp^*Mo(CO)_2(\eta^2\text{-}C_{60})\}^-$ (**3**) containing cyclopentadienyl (**1**, **2**) and pentamethylcyclopentadienyl (**3**) molybdenum dicarbonyl η^2-coordinated to fullerenes have been obtained by the reaction of the $(PPN^+)(fullerene^{\bullet-})$ salt with the $\{Cp^{(*)}Mo(CO)_{3(2)}\}_2$ dimers (PPN^+ is bis(triphenylphosphoranylidene)ammonium cation). The $\{CpMo(CO)_2(\eta^2\text{-}C_{60(70)})\}^-$ anions contain neutral C_{60} and C_{70}. Optical properties and geometry of the $CpMo(CO)_2$ moieties in **1** and **2** are also similar to those in $(PPN^+)\{CpMo^0(CO)_3\}^-$. The analysis of optical data for **3** shows that η^2-coordinated C_{60} molecules are more negatively charged in **3** than in **1** and **2**. Complexes **1**-**3** show weak EPR signals indicating that most part of the samples is EPR silent and diamagnetic. Diamagnetism of the anions in **1**-**3** is explained by the chemical bond formation between initially paramagnetic $CpMo^I(CO)_2$ and $(fullerene)^{\bullet-}$ units. The DFT calculations for **1** and **3** support the diamagnetic singlet ground state for both complexes, in which the singlet-triplet energy gaps calculated at the M11/cc-pVTZ-PP/cc-pVDZ level of theory are about 1.27 and 0.95 eV, respectively. According to the calculations, C_{60} molecules are more negatively charged in **3** than in **1** and that can be explained by stronger back donation from the molybdenum moieties to fullerenes.

Introduction

Fullerenes are widely used in the design of magnetic and conducting compounds[1-4]. Transition metal complexes of fullerenes are also of special interest[5-10] since metals affecting electronic structure and properties of fullerenes can provide compounds with promising properties. Coordination complexes of fullerenes were obtained with palladium, iridium, nickel, cobalt, ruthenium, rhodium and some other metals. It was shown that metals generally coordinate to the 6-6 bonds of C_{60} by η^2-type.[5-10] One fullerene molecule can coordinate from one to six metal centers[6, 11, 12], as well as metal-bridged fullerene dimers[13, 14] and even polymers[15] were obtained. Metal-centered free radicals $[CpM(CO)_3]^{\bullet}$ generated photochemically from the $\{CpM(CO)_3\}_2$ dimers (M = Cr, Mo) also coordinate to fullerenes C_{60} and C_{70} and single-wall carbon nanotubes to form EPR active radical adducts.[16, 17] Similarly metal-centered radicals formed from $Re_2(CO)_{10}$ and $\{CpRu(CO)_2\}_2$ in thermal or photolytic conditions add to C_{60} to form coordination complexes $\{Re(CO)_5\}_2(C_{60})$[18] and $\{\eta^1\text{–}CpRu(CO)_2\}_2(C_{60})$[19]. Potentially charge transfer from metal to fullerene can provide high conductivity at appropriate packing of fullerene anions in a crystal. Though metals in zero oxidation state show relatively strong donor properties, no charge transfer was found in the transition metal fullerene complexes.[5-15] Anionic fullerene complexes with metal carbonylates are also known: $(PPN^+)\{Co(CO)_3(\eta^2\text{–}C_{60})\}^-$, $(PPN^+)\{M(CO)_4(\eta^2\text{–}C_{60})\}^-$ (M = Mn and Re) and $(PPN^+)\{CpM(CO)_2(\eta^2\text{–}C_{60})\}^-$ (M = Mo and W) (PPN^+ is bis(triphenylphosphoranylidene)ammonium cation).[20-23] Similar anionic complexes were obtained with fullerene C_{70} and higher fullerenes.[21] However, in spite of that coordination units with fullerenes are negatively-charged, fullerenes are neutral in these complexes, and negative charge is localized mainly on the metal-containing fragments, such as

$\{Mn(CO)_4\}^-$ or $\{CpM(CO)_2\}^-$. This conclusion was derived based on the absence of the absorption bands of C_{60}^- in the solution NIR spectra of the complexes.[20-23]

Recently,[24] we have obtained two anionic coordination complexes of iridium(II) pentamethylcyclopentadienyl chloride and iodide with fullerene C_{60}: $(TBA^+)\{(Cp^*IrCl)(\eta^2\text{–}C_{60})\}^-$ and $(TBA^+)\{(Cp^*IrI)(\eta^2\text{–}C_{60})\}^-$ (TBA^+ is tetrabutylammonium cation). These complexes were obtained via the reaction of the $(TBA^+)(C_{60}^{\bullet-})$ salt with $Cp^*Ir^{II}X$ (X = Cl, I) and as was shown by optical spectra, the η^2–coordinated fullerenes are negatively charged in these complexes.[24] We suppose that transition metal compounds with donor Cp* ligand in combination with fullerene radical anions can yield coordination complexes with even ionized C_{60}^- which have been studied very weakly by now.

In this work, we perform the reaction of the $C_{60}^{\bullet-}$ and $C_{70}^{\bullet-}$ radical anions with the pentamethylcyclopentadienyl molybdenum dicarbonyl dimers, $\{Cp^*Mo(CO)_2\}_2$, and, for comparison, with the $\{CpMo(CO)_3\}_2$ dimers containing cyclopentadienyl ligand. Previously anionic $(PPN^+)\{CpMo(CO)_2(\eta^2\text{-}C_{60})\}^-$ and $(PPN^+)\{CpMo(CO)_2(\eta^2\text{-}C_{70})\}^-$ complexes were obtained as powders and characterized by electrospray mass, solution IR and NIR spectra, and ^1H and ^{13}C NMR spectra.[22, 23] We obtained complexes $(PPN^+)\{CpMo(CO)_2(\eta^2\text{-}C_{60})\}^-$ (**1**) and $(PPN^+)\{CpMo(CO)_2(\eta^2\text{-}C_{70})\}^-\cdot 0.5C_6H_{14}$ (**2**) as single crystals and analyzed their crystal structures and solid-state IR, visible-NIR and EPR spectra. Moreover, we obtained new complex $(PPN^+)\{Cp^*Mo(CO)_2(\eta^2\text{-}C_{60})\}^-\cdot C_6H_5CN\cdot C_6H_4Cl_2$ (**3**) and found that η^2-coordinated C_{60} is more negatively charged in **3** than in **1** and **2**. We present crystal and molecular structures of **1**-**3** and their solid-state IR, UV-visible-NIR and EPR spectra. DFT calculations for **1** and **3** were carried out. Reference compound $(PPN^+)\{CpMo^0(CO)_3\}^-$ (**4**) was also crystallized and its reaction with C_{60} was studied.

Results and discussion

a). Synthesis

Reaction Scheme:

$(PPN^+)(C_{60}^{\bullet-}) + \{CpMo^I(CO)_3\}_2 \longrightarrow (PPN^+)\{CpMo(CO)_2(\eta^2\text{-}C_{60})\}^-$ (1)

$(PPN^+)(C_{70}^{\bullet-}) + \{CpMo^I(CO)_3\}_2 \longrightarrow (PPN^+)\{CpMo(CO)_2(\eta^2\text{-}C_{70})\}^-$ (2)

$(PPN^+)(C_{60}^{\bullet-}) + \{Cp^*Mo^I(CO)_2\}_2 \longrightarrow (PPN^+)\{Cp^*Mo(CO)_2(\eta^2\text{-}C_{60})\}^-$ (3)

$(PPN^+)(C_{60}(CF_3)_{12}^{\bullet-}) + \{CpMo^I(CO)_3\}_2 \longrightarrow (PPN^+)\{CpMo^0(CO)_3\}^-$ (**4**)

$(PPN^+)(Cl^-) + (Na^+)(Fluorenone^{\bullet-}) + \{CpMo^I(CO)_3\}_2$

$(PPN^+)\{CpMo^0(CO)_3\}^-$ (4) + $C_{60} \longrightarrow (PPN^+)\{CpMo(CO)_2(\eta^2\text{-}C_{60})\}^-$ (1)

$(PPN^+)(Cl^-) + (Na^+)(Fluorenone^{\bullet-}) + \{Cp^*Mo^I(CO)_2\}_2 \not\longrightarrow$

$(PPN^+)\{Cp^*Mo^0(CO)_2\}^-$ (not formed)

The reactions carried out to prepare **1**-**4** are shown in Scheme. The $\{CpMo(CO)_3\}_2$ and $\{Cp^*Mo(CO)_2\}_2$ dimers are bonded by a triple Mo≡Mo bond.[25] Formal charge on molybdenum atoms in these dimers should be I to compensate negative −1 charge of the Cp(*) ligand. Fullerene radical anions interacting with the dimers split the metal-metal bonds and coordinate to the $Cp^{(*)}Mo(CO)_2$ moieties forming anionic $(PPN^+)\{Cp(*)Mo(CO)_2(\eta^2\text{-}C_{60(70)})\}^-$ complexes. In this case the PPN^+ cations compensate negative −1 charge of the $Cp^{(*)}$ ligand. However, the distribution of charges between molybdenum and fullerene should depend on their redox properties. We found that the $\{CpMo(CO)_3\}_2$ dimers can be reduced by sodium fluorenone ketyl in the presence of PPN^+, and the crystals of $(PPN^+)\{CpMo^0(CO)_3\}^-$ (**4**) were obtained from this solution. On the contrary, the $\{Cp^*Mo(CO)_2\}_2$ dimers cannot be reduced by sodium fluorenone ketyl ($E^{-/0} = -1.3$ V in CH_2Cl_2)[26] in the presence of PPN^+. As a result, we expected that the coordinated $CpMo(CO)_2$ moieties are more easily reduced in comparison with $Cp^*Mo(CO)_2$.

We found that the reaction of the $(PPN^+)(C_{60}^{\bullet-})$ salt with the $\{CpMo(CO)_3\}_2$ dimers as well as the reaction of neutral C_{60} with the $(PPN^+)\{CpMo(CO)_3\}^-$ salt finally yields isostructural crystals of $(PPN^+)\{CpMo(CO)_2(\eta^2\text{-}C_{60})\}^-$ (**1**, see Scheme). However, higher quality crystals were obtained for the former reaction route through $(PPN^+)(C_{60}^{\bullet-})$. It should be noted that the latter reaction route was used successfully previously for the preparation of a series of anionic coordination complexes: $(PPN^+)\{Co(CO)_3(\eta^2\text{–}C_{60})\}^-$, $(PPN^+)\{M(CO)_4(\eta^2\text{–}C_{60})\}^-$ (M = Mn and Re) and $(PPN^+)\{CpM(CO)_2(\eta^2\text{–}C_{60})\}^-$ (M = Mo and W).[20-23]

b). Optical properties

The spectra of **1**-**3** in KBr pellets (Fig. 1) in the UV-visible-NIR range allow the estimation of charge state of fullerenes in these complexes. Intense bands in the spectrum of **1** at 452 and 715 nm (Fig. 1a) are attributed to charge transfer from metal to fullerene. Similar bands are observed in all neutral transition metal C_{60} complexes.[5-10] A weak band at 1064 nm (Fig. 1a, arrow) can be attributed to $C_{60}^{\bullet-}$ since the $C_{60}^{\bullet-}$ salts show two bands in the NIR range at 930-950 and a more intense band at 1060-1080 nm.[27, 28] However, the weakness of this band indicates that the $C_{60}^{\bullet-}$ radical anions can be present in **1** only in very small amount as impurity. The spectrum of **2** with C_{70} shows similar bands in the visible range with maxima at 475 and 838 nm (Fig. 1b). As in **1** these bands can also be attributed to charge transfer from metal to fullerene. The $C_{70}^{\bullet-}$ radical anions have a characteristic band in the solid-state NIR spectrum at 1370 nm.[25, 26] The absence of this band in the spectrum of **2** justifies neutral state of C_{70}. Intense absorption bands attributed to charge transfer from metal to neutral fullerene in the spectra of **1** and **2** are not found in the spectrum of **3**. Instead of that only a weak band with maximum at 620 nm is observed which was ascribed to the symmetry forbidden HOMO-LUMO transitions in C_{60}. Coordination complexes with neutral C_{60} as well as **1** and **2** have green color in solution and solid state,[5-10] whereas complex **3** has violet color in both states. Similarly anionic $(TBA^+)\{(Cp^*IrCl)(\eta^2\text{–}$

C_{60})}$^-$ and (TBA$^+$){(Cp*IrI)(η^2–C_{60})}$^-$ complexes containing C_{60} has the F_{1u}(4) mode which is sensitive to charge state of C_{60} and

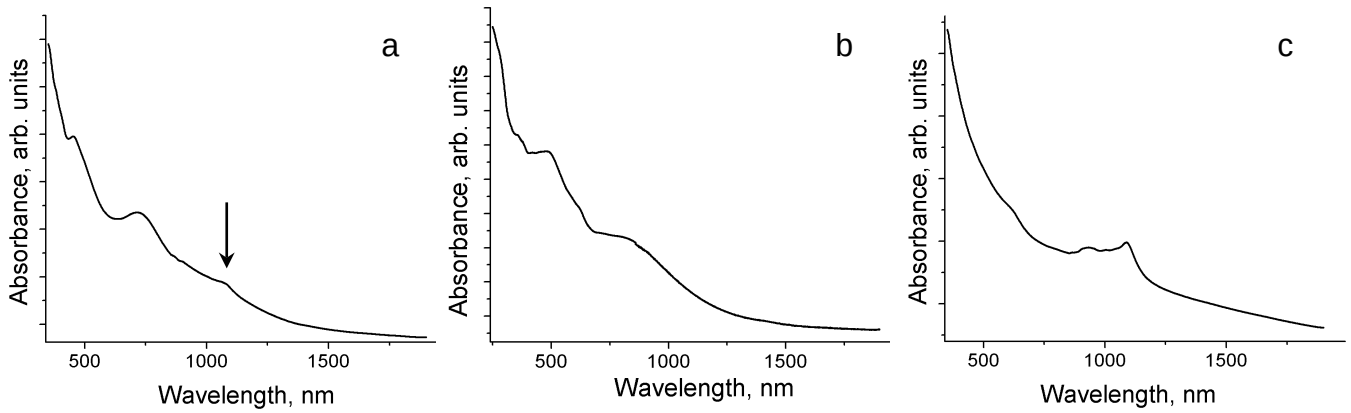

Fig. 1 Spectra of **1** (a), **2** (b) and **3** (c) measured in KBr pellets prepared in anaerobic conditions.

negatively charged C_{60} have also violet color.[24] The bands in the NIR spectrum of **3** at 936 and 1088 nm were attributed to negatively charged C_{60}.

The IR-spectra of **1**-**3** are given in Supporting information (Figs. S1-S4 and Table S1). The spectra are a superposition of absorption bands of fullerenes, cyclopentadienyl (pentamethylcyclopentadienyl) molybdenum dicarbonyl moieties and solvent molecules. Fullerene shifts from 1429 cm^{-1} in neutral state to 1388-1396 cm^{-1} in radical anion state.[27, 28] The band of the F_{1u}(4) mode in the spectrum of **1** is observed at 1416 cm^{-1}. Generally, transition metal complexes with neutral C_{60} manifest these bands at 1416-1420 cm^{-1} and their shift relatively to 1429 cm^{-1} was attributed to π-back donation.[8,10,13-15] C_{70} complex **2** shows the band at 1426 cm^{-1} (this band is only slightly shifted relative to the band of neutral C_{70} at 1429 cm^{-1}). The main band of the C_{60} F_{1u}(4) mode is manifested in the spectrum of **3** at 1392 cm^{-1} and this position indicates that the C_{60} molecules are more negatively charged in **3** than in **1** and **2**, whereas the band at 1412 cm^{-1} which can be attributed to neutral C_{60} is very weak in the spectrum of **3**. Thus, optical spectra in the visible-NIR and IR ranges indicate neutral state of fullerenes in **1** and **2,** whereas fullerene C_{60} is more negatively charged in **3**.

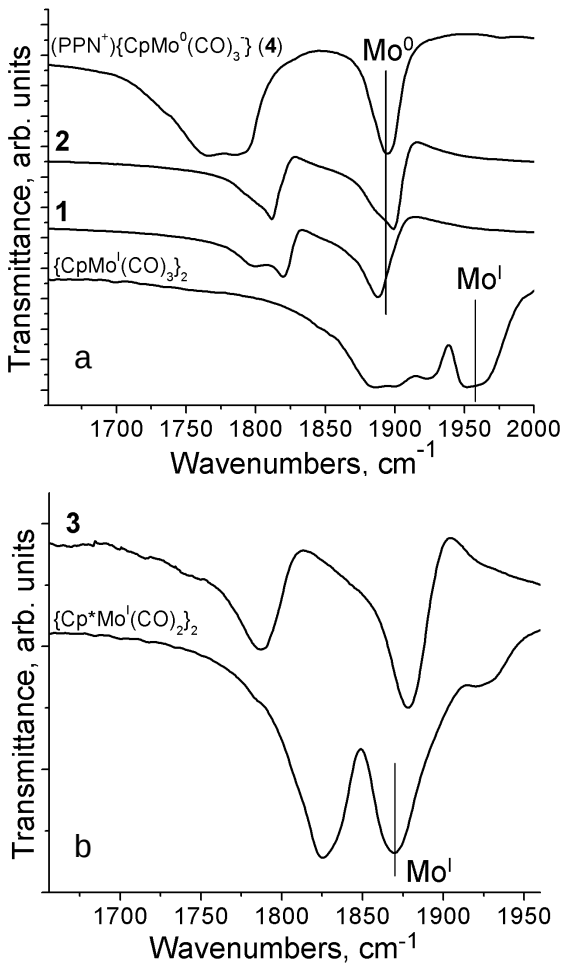

Fig. 2 The position of the absorption bands of the CO stretching mode: (a) the reference compound (PPN$^+$){CpMo^0(CO)$_3$}$^-$ (**4**), the {CpMo^I(CO)$_3$}$_2$ dimer and complexes **1** and **2**; (b) the {Cp*Mo^I(CO)$_2$}$_2$ dimer and complex **3**.

The CO stretching modes of the carbonyls of Cp$^{(*)}$Mo(CO)$_{2\text{-}3}$ are very sensitive to the charge state of molybdenum since the reduction of the {CpMo^I(CO)$_3$}$_2$ dimers to (PPN$^+$){CpMo^0(CO)$_3$}$^-$ results in the shift of higher-frequency CO band from 1953 to 1895 cm^{-1} (the shift is 58 cm^{-1}, Fig. 2a). The position of this mode in the spectra of **1** and **2** is at 1888 and 1898 cm^{-1}, respectively (Fig. 2a). This position is close to that in the spectrum of (PPN$^+$){CpMo^0(CO)$_3$}$^-$. The IR spectra of starting {Cp*Mo(CO)$_2$}$_2$ dimers and **3** in the 1600-2000 cm^{-1} range are shown in Fig. 2b. The dimers have the position of higher-frequency CO band at 1870 cm^{-1} and this band is only slightly shifted to 1878 cm^{-1} at the formation of **3**. Therefore, the charged state of molybdenum in **3** should be closer to that in starting {Cp*Mo(CO)$_2$}$_2$ dimers.

c). Crystal structures

Molecular structure of the {Cp$^{(*)}$Mo(CO)$_2$(η^2-$C_{60(70)}$)}$^-$ anions in **1**-**3** and the {CpMo(CO)$_3$}$^-$ anion in **4** are shown in Fig. 3. The average bond lengths in these anions are listed in Table 1. Molybdenum is η^2-coordinated to the 6-6 bonds of C_{60} as well as the bond between two hexagons in C_{70}. The Mo-C(fullerene) bond length is close to 2.25 Å in **1** and **2** and 2.28 Å in **3** (Table 1). The Mo-C(fullerene) bond lengths in **1**-**3** are close to those

Table 1. Geometric parameters for reference molybdenum compounds and coordination complexes of $Cp^{(*)}Mo(CO)_2$ with fullerenes C_{60} and C_{70} (**1-3**).

Compound	Average length of main bonds, Å					
	Mo-C(CO)	CO	Mo-C(Cp)	Mo-Cp plane	Mo-C (fullerene)	coord 6-6 bond/ adjacent 6-5
$CpMo^{II}(CO)_3Cl$[29]	2.000(2)	1.139(2)	2.280(2)	1.986	-	-
$\{CpMo^{I}(CO)_3\}_2$[25]	1.977(3)	1.148(3)	2.338(3)	-	-	-
$\{Cp^*Mo^{I}(CO)_2\}_2$[30]	2.10(2)	1.12(2)	2.29(2)	1.99	-	-
$(PPN^+)\{CpMo^0(CO)_3\}^-$ (**4**)	1.934(2)	1.170(2)	2.386(2)	2.065	-	-
$(PPN^+)\{CpMo^0(CO)_2(\eta^2\text{-}C_{60})\}^-$ (**1**)	1.945(3)	1.160(3)	2.367(3)	2.036	2.246(2)	1.497(4)/1.479(3)
$(PPN^+)\{CpMo^0(CO)_2(\eta^2\text{-}C_{70})\}^-$ (**2**)	1.934(7)	1.165(7)	2.337(5)	2.000	2.252(6)	1.510(8)/1.471(8)
$(PPN^+)\{Cp^*Mo^{I}(CO)_2(\eta^2\text{-}C_{60}^-)\}^-$ (**3**)[a]	1.934(8)	1.18(1)	2.402(3)	2.071	2.282(7)	1.483(11)/1.491(10)

[a] Geometry was determined for major orientation.

in other coordination fullerene complexes with molybdenum (2.27-2.37 Å)[31-33].

The 6-6 bonds which the molybdenum atoms are coordinated to are noticeably elongated to 1.497(4) and 1.483(11) Å in **1** and **3**, whereas the average length of other 6-6 bonds in C_{60} is 1.389(4) Å. Similarly, the 5-6 bonds of C_{60} adjacent to the 6-6 bond involved in the coordination are elongated from the average value of 1.450(4) to 1.479(4) and 1.491(10) Å in **1** and **3**, respectively. Similarly, the bond between two hexagons in C_{70} which the molybdenum atom is coordinated to is elongated in **2** from the average value of 1.390(8) to 1.510(8) Å. All these effects can be attributed to the π-back donation[5-10].

Formal oxidation state of molybdenum affects molecular geometry of the $CpMo(CO)_3$ units. For example, the Mo-C(CO) bonds are elongated in the following row: $(PPN^+)\{CpMo^0(CO)_3\}^-$ < $\{CpMo^{I}(CO)_3\}_2$ < $CpMo^{II}(CO)_3Cl$ (Table 1), and carbonyl and the Mo-C(Cp) bonds are noticeably shortened in this sequence (Table 1). The lengths of these bonds in **1** and **2** are closer to those in $(PPN^+)\{CpMo^0(CO)_3\}^-$ than to the lengths of these bonds in starting $\{CpMo^{I}(CO)_3\}_2$ (Table 1). The $Cp^*Mo(CO)_2$ moieties have different lengths of the main bonds in the starting dimers and in **3**. However, the geometry of $\{Cp^*Mo(CO)_2\}_2$ dimers was determined previously with a very large error (3σ = 0.06 Å).

The view on the crystal structure of **1** is shown in Fig. 4. In spite of the presence of coordination groups, closely packed strongly corrugated C_{60} layers are formed. Large vacancies formed in fullerene layers due to corrugation accommodate the PPN^+ cations (Fig. 4b). The center-to-center (ctc) interfullerene distances are equal to 9.96 Å along the *b* direction and 9.95 Å along the *c* direction. Since these distances are essentially shorter than the van der Waals diameter of C_{60} (10.18 Å), multiple van der Waals C…C contacts are formed between fullerenes in the layers (2.97-3.38 Å, Fig. 4a). Similar corrugated fullerene layers are formed in anionic $(PPN^+)\{Mn(CO)_4(\eta^2\text{-}C_{60})\}^-$. In this case the ctc interfullerene distances are equal to 9.89 and 10.00 Å.[22]

The structure of complex **2** with fullerene C_{70} is also layered. In the structure, closely packed layers formed by $\{CpMo(CO)_2(\eta^2\text{-}C_{70})\}^-$ anions alternate with the layers formed by PPN^+ cations and hexane molecules. Within the fullerene

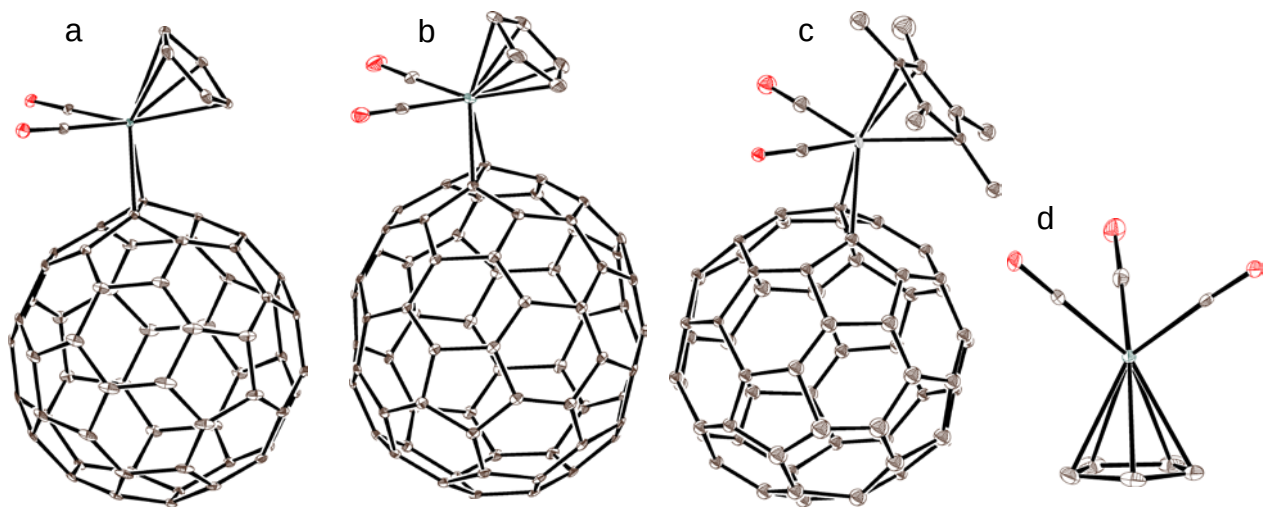

Fig. 3 Molecular structure of the studied anions: (a) $\{CpMo(CO)_2(\eta^2\text{-}C_{60})\}^-$ in **1**; (b) $\{CpMo(CO)_2(\eta^2\text{-}C_{70})\}^-$ in **2**; (c) $\{Cp^*Mo(CO)_2(\eta^2\text{-}C_{60})\}^-$ in **3** (only major orientation of this anion is shown) and (d) $\{CpMo(CO)_3\}^-$ in **4**. The PPN^+ cations and solvent molecules are not shown. Ellipsoid probability is 20%.

layers, closely packed uniform linear chains composed of the $\{CpMo(CO)_2(\eta^2\text{-}C_{70})\}^-$ anions can be outlined along the *a* axis (Fig. 5a). The distance between the center of mass of C_{70}

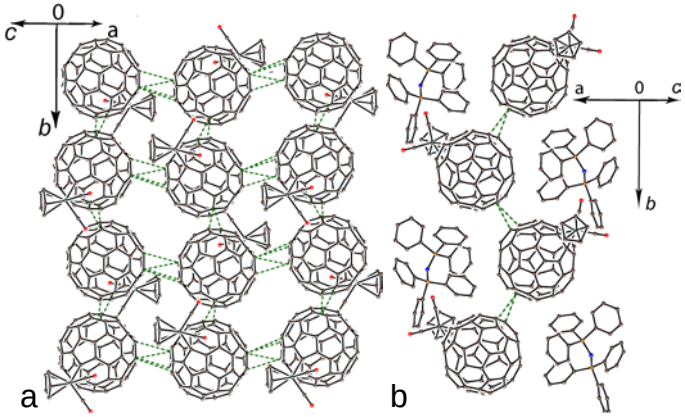

Fig. 4 View on anionic $\{CpMo(CO)_2(\eta^2\text{-}C_{60})\}^-$ layer in **1** (a) and view along this layer (b). Short van der Waals C···C contacts are shown by green dashed lines.

spheroids is 9.98 Å and each anion forms four van der Waals C…C contacts with the neighbors in the 3.19-3.37 Å range (these contacts are shown by green dashed lines in Fig. 5a). The distance between the center of mass of two C_{70} spheroids from different chains is 10.67 Å and the C···C contacts do not form. Fullerene layers are also strongly corrugated in **2** producing vacancies for the PPN^+ cations (Fig. 5b).

Complex **3** contains zigzag chains from the $\{Cp^*Mo(CO)_2(\eta^2\text{-}C_{60})\}^-$ anions arranged along the *c* axis (Fig. S5 in Supporting information). The chains are completely isolated by bulky PPN^+ cations and solvent molecules. The ctc interfullerene distances in the chains are not uniform alternating between 9.89 and 10.06 Å (van der Waals C···C contacts are 3.12-3.39 Å).

Crystal structure of **4** is shown in Fig. S6 of Supporting information. The $\{CpMo(CO)_3\}^-$ anions form pairs with short O(CpMo(CO)$_3$)…C(Cp ligand of CpMo(CO)$_3$) contacts.

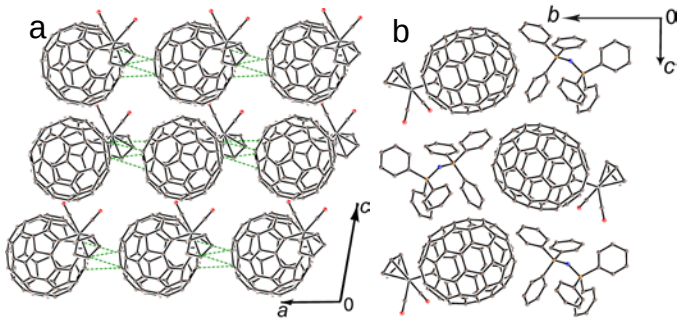

Fig. 5 View on anionic $\{CpMo(CO)_2(\eta^2\text{-}C_{70})\}^-$ layers (a) and along these layers (b) in **2**. Short van der Waals C···C contacts are shown by green dashed lines.

d). Magnetic properties

Magnetic properties of **1-3** were studied by EPR and SQUID measurements. A weak EPR signal manifested by complex **1** can be approximated by broad and narrow Lorentzian lines with g_1 = 1.9983 and linewidth of ΔH = 4.47 mT and g_2 = 2.0003 and ΔH = 0.20 mT at room temperature (295 K). Integral intensity of the narrow line is about 6% of that of the broad line. The narrow line has nearly temperature independent linewidth and *g*-factor down to 4 K. The broad line strongly narrows with the temperature decrease as generally observed for the EPR signals from $C_{60}^{\bullet-}$.[25] According to SQUID measurements, only about 2% is S = 1/2 spins per formula unit contribute to the magnetic susceptibility of **1**. We suppose that the observed EPR signals originate mainly from paramagnetic impurities and major part of the sample is EPR silent and diamagnetic.

Complex **2** with C_{70} manifests a very weak EPR signal with g = 2.0008 and linewidth of 0.62 mT at RT. In this case, less than 0.4% of the sample contributes to the EPR signal and **2** is also EPR silent and diamagnetic. The data obtained for **1** and **2** are in a good agreement with optical and X-ray diffraction data showing the presence of neutral fullerenes.

Complex **3** shows the EPR signal approximated well by one Lorentzian line with g = 1.9986 and ΔH = 5.12 mT at RT. The signal of **3** strongly narrows and *g*-factor shifts to smaller values with the temperature decrease. The signal is split into broader and narrower lines below 140 K which have g_1= 1.9974 and ΔH = 3.33 mT and g_2 = 1.9991 and ΔH = 0.94 mT (140 K). The lines narrow below 140 K and their *g*-factors shift to smaller values (Fig. S7 in Supporting information). According to SQUID measurements, only about 4.2% is S = 1/2 spins per formula unit contribute to the magnetic susceptibility of the sample. Therefore, we suppose that the observed EPR signals can originate from paramagnetic impurities, whereas major part of the sample is EPR silent and diamagnetic. Complex **3** is formed by initially paramagnetic $Cp^*Mo^I(CO)_2$ and $C_{60}^{\bullet-}$ species and charges on these species are preserved at the formation of **3** as was concluded from the optical spectra. However, the resulted $\{Cp^*Mo^I(CO)_2(\eta^2\text{-}C_{60}^-)\}^-$ anions can become diamagnetic due to the formation of a coordination bond between $Cp^*Mo^I(CO)_2$ and $C_{60}^{\bullet-}$. Previously, it was even shown that complexes $(TBA^+)\{(Cp^*IrX)(\eta^2\text{-}C_{60})\}^-$ (X = Cl, I) were also EPR silent due to the formation of a coordination bond between fullerene and iridium though they were formed by initially paramagnetic $Cp^*Ir^{II}X$ and $C_{60}^{\bullet-}$ species.[22] Similar diamagnetic state was found for the complexes of cobalt(II) tetraphenyl- or octaethylporphyrins (Co^{II}TPP and Co^{II}OEP) with $C_{60}^{\bullet-}$ and $C_{60}(CN)_2^{\bullet-}$.[32-35] While both porphyrins and fullerene radical anions have paramagnetic ground state with S = 1/2 spin state, the formation of coordination Co(porphyrin)-C(fullerene$^-$) bonds of 2.28-2.32 Å length between them results in diamagnetism and EPR silence of the $\{Co^{II}TPP(C_{60})\}^-$, $[Co^{II}TPP\{C_{60}(CN)_2\}]^-$ and $\{Co^{II}OEP\ (C_{60})\}^-$ anions.[34-37]

e). Theoretical analysis

To obtain the further insights into the electronic structure of the $\{Cp^{(*)}Mo(CO)_2(\eta^2\text{-}C_{60})\}^-$ anions, theoretical analyses at the CAM-B3LYP-D3 and M11/cc-pVTZ-PP/cc-pVDZ levels of theory were performed upon the optimized and unoptimized X-ray structures of **1** and **3**. The total and relative energies, $<S^2>$ values, and number of imaginary frequencies are summarized

in Table S2 of Supporting information. Since both CAM-B3LYP-D3 and M11 functionals afforded nearly the same results, the results based on the M11 functional are described hereinafter. On the basis of $<S^2>$ values, the spin contamination is nearly negligible for the calculated triplet states because the $<S^2>$ values for the pure triplet state are equal to 2. The closed-shell singlet states are energetically more stable by 1.27 and 0.95 eV than the triplet ones for the $\{CpMo(CO)_2(\eta^2\text{-}C_{60})\}^-$ and $\{Cp^*Mo(CO)_2(\eta^2\text{-}C_{60})\}^-$ anions, respectively, and it is not possible to attain the corresponding triplet state via thermal excitation. Therefore, the present DFT analysis support the diamagnetic nature of $\{CpMo(CO)_2(\eta^2\text{-}C_{60})\}^-$ and $\{Cp^*Mo(CO)_2(\eta^2\text{-}C_{60})\}^-$ observed in the EPR and SQUID measurements. The geometry optimization in the singlet states of $\{Cp^{(*)}Mo(CO)_2(\eta^2\text{-}C_{60})\}^-$ well reproduces the X-ray structure, indicating that the present functional is highly reliable in describing the discussed anions (Fig. 6 and Tables S3, S4 and Fig. S8).

The energy diagrams for the frontier Kohn-Sham orbitals of the singlet states in the geometry-optimized $\{Cp^{(*)}Mo(CO)_2(\eta^2\text{-}C_{60})\}^-$ anions are shown in Figs. 7, S9, and S10. The electronic structures of these complexes resemble each other. The highest occupied molecular orbital (HOMO) is formed by the bonding interaction between the molybdenum-*d* and C_{60}-π orbitals, and (HO−1) and (HO−2)MOs are π bonding orbitals between the molybdenum-*d* and CO-π* antibonding orbitals, indicating the π back-bond. The lowest unoccupied molecular orbitals (LUMO) and (LU+1)MO are localized on the C_{60} moiety.

To further evaluate the bonds around the central molybdenum, Wiberg bond indices (WBIs)[38] were also estimated and summarized in Tables S3 and S4. The sums of WBIs for the two Mo−C bonds with fullerene C_{60} in $\{CpMo(CO)_2(\eta^2\text{-}C_{60})\}^-$ and $\{Cp^*Mo(CO)_2(\eta^2\text{-}C_{60})\}^-$ seem to be in the range of single bond, indicating the generation of diamagnetic species associated with the chemical bond formation. The calculated charge densities are summarized in Tables 2 and S6, and the electrostatic potential maps are shown in Fig. S11. The molybdenum atom and the C_{60} moiety are more positively and negatively charged, respectively, in $\{Cp^*Mo(CO)_2(\eta^2\text{-}C_{60})\}^-$ (**3**) than those in $\{CpMo(CO)_2(\eta^2\text{-}C_{60})\}^-$ (**1**). That supports the data of optical spectra showing the more negatively charged C_{60} in **3**.

Considering the bond lengths and WBIs, the Mo−CO and CO bonds in $\{Cp^*Mo(CO)_2(\eta^2\text{-}C_{60}^-)\}$ are stronger and weaker, respectively, than those in $\{CpMo(CO)_2(\eta^2\text{-}C_{60})\}^-$. This is because the contribution of π back-donation from the molybdenum-*d* to CO-π* antibonding orbital in $\{Cp^*Mo(CO)_2(\eta^2\text{-}C_{60})\}^-$ is larger than that in $\{CpMo(CO)_2(\eta^2\text{-}C_{60})\}^-$, which strengthens the Mo−CO π back-bond and weakens the CO bonds. The larger contribution of π back-donation is also justified by the more negatively charged CO ligands in $\{Cp^*Mo(CO)_2(\eta^2\text{-}C_{60})\}^-$ (Tables 2 and S6). The observed and calculated frequencies of CO stretching mode are shown in Tables 3 and S7. The CO stretching modes with higher frequencies at 1888 and 1878 cm^{-1} are predicted at 1877 and 1866 cm^{-1}, respectively, supporting the weakened CO bond in $\{Cp^*Mo(CO)_2(\eta^2\text{-}C_{60}^-)\}$ due to the π back-donation. According to the calculations, more negatively charged C_{60} in **3** than in **1** can be explained by stronger back donation due to the stronger electron donor ligand Cp* in the former case. Thus, the difference in the charge distribution in the $\{CpMo(CO)_2(\eta^2\text{-}C_{60})\}^-$ and $\{Cp^*Mo(CO)_2(\eta^2\text{-}C_{60})\}^-$ anions originates from the different donor strength of the Cp and Cp* ligands and can support the experimental results.

In order to explore the possibility of triplet state, the geometry optimization of triplet state in $\{Cp^*Mo(CO)_2(\eta^2\text{-}C_{60})\}^-$ was carried out. The conformation of the triplet state is different from the singlet one with regard to the coordination manner between $Mo(CO)_2$ and C_{60} moieties, in which the rotation is induced about the Mo−C_{60} bond (Table S5, and Figs. 6 and S8). This geometrical change is accompanied by electron

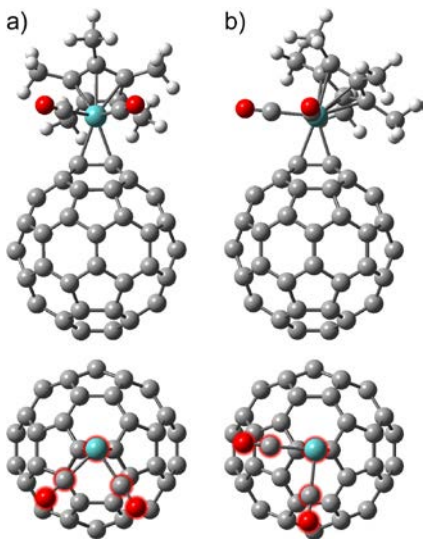

Fig. 6 Optimized structures of the (a) ^1A and (b) ^3A states in $\{Cp^*Mo(CO)_2(\eta^2\text{-}C_{60})\}^-$ at the M11/cc-pVTZ-PP/cc-pVDZ level of theory. In the top view, the Cp* ligands are omitted, and the $Mo(CO)_2$ moiety is highlighted for clarity.

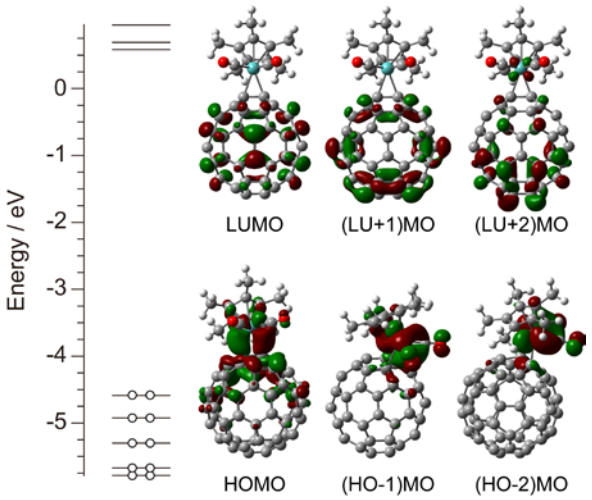

Fig. 7 Energy diagram for the frontier Kohn-Sham orbitals of the ^1A state in $\{Cp^*Mo(CO)_2(\eta^2\text{-}C_{60})\}^-$ calculated at the RM11/cc-pVTZ-PP/cc-pVDZ level of theory.

Table 2. Sum of charge densities for the ^1A states in $\{CpMo(CO)_2(\eta^2\text{-}C_{60})\}^-$ and $\{Cp^*Mo(CO)_2(\eta^2\text{-}C_{60})\}^-$ by Mulliken and natural population analyses at the RM11/cc-pVTZ-PP/cc-pVDZ level of theory[a].

	Mulliken	NPA[b]
$\{CpMo(CO)_2(\eta^2\text{-}C_{60})\}^-$		
Mo1	−0.469	−0.916
C66−O1	0.112	0.284
C67−O2	0.112	0.284
Cp	0.044	−0.005
C_{60}	−0.799	−0.648
$\{Cp^*Mo(CO)_2(\eta^2\text{-}C_{60})\}^-$		
Mo1B	−0.373	−0.842
C11B−O1B	0.096	0.268
C12B−O2B	0.106	0.286
Cp*	0.042	−0.020
C_{60}	−0.869	−0.692

[a] Geometry optimization was carried out.

[b] Natural population analysis.

Table 3. Observed and calculated frequencies (cm^{-1}) of CO stretching mode of the ^1A states in $\{CpMo(CO)_2(\eta^2\text{-}C_{60})^-\}$ and $\{Cp^*Mo(CO)_2(\eta^2\text{-}C_{60}^-)\}$ at the RM11/cc-pVTZ-PP/cc-pVDZ level of theory.

Obs.	RM11[a]
$\{CpMo(CO)_2(\eta^2\text{-}C_{60})\}^-$	
1798	1822
1819	1877
1888	
$\{Cp^*Mo(CO)_2(\eta^2\text{-}C_{60})\}^-$	
1787	1808
1878	1866

[a]The calculated frequencies are scaled by 0.9244.

transfer from $Cp^*Mo(CO)_2$ to the C_{60} moiety (Table S6 and Fig. S11), and results in a resurgence of spin densities on molybdenum and C_{60} moiety (Table S8 and Fig. S12). From another point of view, this result suggests that the spin state is controllable by tuning the conformation chemically and/or physically (e.g. ligand design, shear stress, photo excitation, and so on).

Experimental

Materials

(PPN)Cl (99%) was purchased from Aldrich. Fullerenes C_{60} (99.9%) and C_{70} (99%) were received from MTR Ltd. The $\{CpMo(CO)_3\}_2$ (> 98%) and $\{Cp^*Mo(CO)_2\}_2$ dimers (> 99%) were purchased from Aldrich and Strem, respectively. Sodium fluorenone ketyl was obtained as described.[10] Solvents were purified under argon atmosphere. *o*-Dichlorobenzene ($C_6H_4Cl_2$) was distilled over CaH_2 under reduced pressure; hexane was distilled over Na/benzophenone, and benzonitrile was distilled over Na under reduced pressure. All operations on the synthesis of air-sensitive **1-4** and their storage were carried out in a MBraun 150B-G glove box under controlled atmosphere with water and oxygen content less than 1 ppm. The solvents were degassed and stored in the glove box. KBr pellets for IR- and UV-visible-NIR measurements were prepared in the glove box. EPR and SQUID measurements were performed on polycrystalline samples of **1-3** sealed in 2 mm quarz tubes under 10^{-5} Torr.

Synthesis

Crystals of **1-4** were obtained by diffusion technique. The reaction solutions were filtered in a 50 mL glass tube of 1.8 cm in diameter with a ground glass plug, and 30 mL of hexane was layered over the solution. The crystals were precipitated during 1-2 months. The solvent was decanted from the crystals and they were washed with hexane. Composition of the complexes was determined from X-ray diffraction of single crystal. Several crystals from the synthesis tested by X-ray diffraction showed the presence of only one crystal phase.

For preparation of $(PPN^+)\{CpMo(CO)_2(\eta^2\text{-}C_{60})\}^-$ (**1**), 30 mg (0.042 mmol) of C_{60} was reduced in 18 mL of *o*-dichlorobenzene/benzonitrile (1:1) mixture with slight excess of sodium fluorenone ketyl (12 mg, 0.059 mmol) in the presence of (PPN)Cl (25 mg, 0.043 mmol) for two hours at 100°C to produce brown-violet solution of the $(PPN^+)(C_{60}^{\bullet-})$ salt. This solution was filtered hot into a flask containing slight excess of the $\{CpMo(CO)_3\}_2$ dimers (12 mg, 0.049 mmol) and the mixture was stirred during four hours at 80°C to give brown-green solution, which was then cooled down to room temperature and filtered into the tube for diffusion. The diffusion into the hexane layer produced black needles in 76% yield.

The crystals of $(PPN^+)\{CpMo(CO)_2(\eta^2\text{-}C_{70})\}^-\cdot 0.5C_6H_{14}$ (**2**) were obtained similarly, but we used C_{70} (35 mg, 0.042 mmol) instead of C_{60}. The deep red solution of the $(PPN^+)(C_{70}^{\bullet-})$ salt was filtered hot into a flask containing slight excess of the $\{CpMo(CO)_3\}_2$ dimers (12 mg, 0.049 mmol), and the mixture was stirred during four hours at 80°C to give deep-red solution. It was cooled down to room temperature and filtered into the tube for diffusion. The diffusion into the hexane layer produced black needles in 62% yield.

The crystals of $(PPN^+)\{Cp^*Mo(CO)_2(\eta^2\text{-}C_{60})\}^-\cdot C_6H_5CN\cdot C_6H_4Cl_2$ (**3**) were obtained similarly to **1**, but we filtered hot brown-violet solution of the $(PPN^+)(C_{60}^{\bullet-})$ salt into a flask containing slight excess of the $\{Cp^*Mo(CO)_2\}_2$ dimers (14 mg, 0.049 mmol), and the mixture was stirred more during four hours at 80°C (brown-violet color of the solution remained unchanged while stirred). It was cooled down to room temperature and filtered into the tube for diffusion. The diffusion into the hexane layer produced black rhombs in 54% yield.

The crystals of $(PPN^+)\{CpMo(CO)_3\}^-$ (**4**) were obtained as a result of the synthesis of the coordination complex with fullerene derivative $C_{60}(CF_3)_{12}$. Initially, we generated green

$(PPN^+)(C_{60}(CF_3)_{12}^{\bullet-})$ salt in pure *o*-dichlorobnezene as described in Ref. 39. The solution was filtered into the flask containing slight excess of $\{CpMo(CO)_3\}_2$. Stirring at 80ºC for 1 hour resulted in the disappearance of green color of the solution characteristic of $C_{60}(CF_3)_{12}^{\bullet-}$, and greenish-yellow solution was formed. Slow mixing with hexane produced well-shaped yellow crystals of **4** in 43% yield. The composition of **4** was determined from X-ray diffraction of single crystal. Finally, we found that similar crystals could be obtained by the reduction of the $\{CpMo(CO)_3\}_2$ dimers (12 mg, 0.049 mmol) by one equivalent of sodium fluorenone ketyl in the presence of (PPN)Cl. Red color of the starting compound disappears under reduction, and yellow-pink solution was formed. The crystals of **4** were precipitated by slow mixing with hexane.

We found that addition of filtered solution of **4** into the flask containing 30 mg of C_{60} results in the dissolution of fullerene, and brown-green solution formed. Slow mixing of the obtained solution with hexane produced the crystals of **1.** The crystals tested by X-ray diffraction were found to be isostructural to **1**. However, the crystals were of lower quality than those obtained via the $(PPN^+)(C_{60}^{\bullet-})$ salt.

Due to high air sensitivity, the composition of **1-4** was determined from X-ray diffraction on single crystals only. Elemental analysis can hardly be used in this case since **1-4** react with oxygen in air prior to quantitative oxidation procedure for analysis.

General

UV-visible-NIR spectra were measured in KBr pellets on a Perkin Elmer Lambda 1050 spectrometer in the 250-2500 nm range. FT-IR spectra were obtained in KBr pellets with a Perkin-Elmer Spectrum 400 spectrometer (400-7800 cm^{-1}). EPR spectra were recorded for sealed polycrystalline samples of **1-3** in the range of 4 − 295 K with a JEOL JES-TE 200 X-band ESR spectrometer equipped with a JEOL ES-CT470 cryostat. The number of spins was estimated from the comparison of integral intensity of the signal with that from the weighted amount of $CuSO_4{\cdot}5H_2O$. A Quantum Design MPMS-XL SQUID magnetometer was used to measure static magnetic susceptibility of **1** and **3** at 100 mT magnetic field in cooling and heating conditions in the 300 − 1.9 K range. A sample holder contribution and core temperature independent diamagnetic susceptibility (χ_d) were subtracted from the experimental values. The χ_d values for the salt was obtained by the extrapolation of the data (30-300 K) in the high-temperature range by fitting the data with the following expression: $\chi_M = C/(T - \Theta) + \chi_d$, where C is Curie constant and Θ is Weiss temperature.

Crystal structure determination

Crystal data of 1 at 100(2) K: $C_{103}H_{35}MoNO_2P_2$, M_r = 1476.20 g mol^{-1}, black plate, monoclinic, $P2_1/c$, a = 21.454(1), b = 16.3401(10), c = 19.8350(8) Å, β = 117.151(3)º, V = 6187.2(5) $Å^3$, Z = 4, d_{calc} = 1.585 g·cm^{-3}, μ = 0.460 mm^{-1}, F(000) = 2992, reflections measured 112100, unique reflections 16770, reflections with $I > 2\sigma(I)$ = 15750, parameters refined 982, restraints 24, R_1 = 0.0516, wR_2 = 0.1269, G.O.F. = 1.006, CCDC 1051550.

Crystal data of 2 at 100(2) K: $C_{116}H_{42}MoNO_2P_2$, M_r = 1639.38 g mol^{-1}, black plate, monoclinic, $P2_1/c$, a = 9.9787(10), b = 41.179(4), c = 17.2206(16) Å, β = 100.917(2)º, V = 6948.1(11) $Å^3$, Z = 4, d_{calc} = 1.567 g·cm^{-3}, μ = 0.303 mm^{-1}, F(000) = 3332, reflections measured 36997, unique reflections 12038, reflections with $I > 2\sigma(I)$ = 6647, parameters refined 1102, restraints 1227, R_1 = 0.0666, wR_2 = 0.1448, G.O.F. = 1.002, CCDC 1043663.

Crystal data of 3 at 120(2) K: $C_{121}H_{54}Cl_2MoN_2O_2P_2$, M_r = 1796.44 g mol^{-1}, black plate, triclinic, $P\bar{1}$, a = 14.0336(4), b = 16.0159(4), c = 18.2067(5) Å, α = 88.962(2), β = 81.128(2), γ = 78.470(2)º, V = 3961.26(19) $Å^3$, Z = 2, d_{calc} = 1.506 g·cm^{-3}, μ = 0.339 mm^{-1}, F(000) = 1832, reflections measured 38286, unique reflections 19105, reflections with $I > 2\sigma(I)$ = 10727, parameters refined 1423, restraints 1464, R_1 = 0.1006, wR_2 = 0.2939, G.O.F. = 0.994, CCDC 1043666.

Crystal data of 4 at 100(2) K: $C_{44}H_{41}MoNO_3P_2$, M_r = 789.66 g mol^{-1}, yellow block, monoclinic, $P2_1/c$, a = 13.927(1), b = 18.956(1), c = 13.7160(10) Å, β = 91.01(1) º, V = 3620.5(4) $Å^3$, Z = 4, d_{calc} = 1.449 g·cm^{-3}, μ = 0.494 mm^{-1}, F(000) = 1632, $2\theta_{max}$ = 58.28º, reflections measured 23396, unique reflections 9500, reflections with $I > 2\sigma(I)$ = 7752, parameters refined 460, R_1 = 0.0313, wR_2 = 0.0822, G.O.F. = 1.008, CCDC 1051551.

The intensity data for **1** were collected on a MAR225 CCD detector using synchrotron radiation at the BESSY storage ring, BL 14.2 (λ = 0.9050 Å, PSF of the Free University of Berlin, Germany). The structures were solved by direct method and refined by the full-matrix least-squares method against F^2 using SHELX-97 package.[40] Data collection for the crystals of **2** and **3** was carried out with a Bruker Smart Apex II CCD diffractometer with graphite monochromated MoK_α radiation using a Japan Thermal Engineering cooling system DX-CS190LD. Raw data reduction to F^2 was carried out using Bruker SAINT.[41] The structure was solved by direct method and refined by the full-matrix least-squares method against F^2 using SHELXL-2013.[40] The intensity data for **4** were collected on an IPDS (Stoe) diffractometer with graphite monochromated MoK_α radiation. Experimental data were processed using X-Area software. The structures were solved by a direct method and refined by a full-matrix least-squares method against F^2 using SHELX-97.[40] All non-hydrogen atoms were refined anisotropically. Positions of hydrogen atoms were included into refinement in a riding model. See …….for crystallographic data in CIF.

The structure of **2** contains hexane molecule disordered between two orientations with the 0.486(8)/0.514(8) occupancies. Two of six phenyl substituents of PPN^+ are disordered between two orientations with the 0.592(14)/0.408(14) and 0.507(8)/0.493(8) occupancies. The structure of **3** has two orientations of the $\{Cp^*Mo(CO)_2(\eta^2\text{-}C_{60})\}^-$ moieties having the 0.621(2)/0.379(2) occupancies. At the same time the PPN^+ cations, solvent C_6H_5CN and $C_6H_4Cl_2$ molecules are completely ordered in **3**. To keep geometry of disordered hexane molecule and two phenyl substituents in

PPN^+ of **2** and the disordered $\{Cp^*Mo(CO)_2(\eta^2\text{-}C_{60})\}^-$ moieties in **3** close to ideal one, restraints were applied for the refinement of the crystal structures of **2** and **3**.

Computational details

Density functional theory (DFT) calculations were carried out by the restricted and unrestricted methods based on CAM-B3LYP-D3 with the Grimme's D3 dispersion[42] and M11.[43] The cc-pVTZ-PP[44] and cc-pVDZ[45] basis sets were used for molybdenum and the other atoms, respectively. In order to ensure reliability of frequencies, both "Opt=Tight" and "Int=Ultrafine" were specified. The stabilities of wave functions were confirmed by specifying the "Stable=Opt" keyword in the present DFT calculations. The subsequent natural bond orbital (NBO) analysis was done by the NBO program.[46] All the computations were performed with the Gaussian 09 program package.[47]

Conclusions

We obtained and structurally characterized anionic coordination complexes of fullerenes C_{60} and C_{70} with cyclopentadienyl (**1**, **2**) and pentamethylcyclopentadienyl (**3**) molybdenum dicarbonyl. Molybdenum is η^2-coordinated to fullerenes. The $\{CpMo(CO)_2(\eta^2\text{-}C_{60(70)})\}^-$ anions contain neutral fullerenes C_{60} and C_{70} in **1** and **2**, whereas fullerenes are more negatively charged in $\{Cp^*Mo^I(CO)_2(\eta^2\text{-}C_{60}^-)\}^-$ (**3**). According to the calculations, the difference in charge distribution in the $\{CpMo(CO)_2(\eta^2\text{-}C_{60})\}^-$ and $\{Cp^*Mo(CO)_2(\eta^2\text{-}C_{60})\}^-$ anions is explained by stronger back donation from the molybdenum moieties to fullerenes in **3** than in **1** originated from the different donor strength of the Cp and Cp* ligands. Thus, additional ligands at the metal centers can influence the charge distribution between metal and fullerene in the coordination complexes and potentially can affect optical, magnetic and conducting properties of transition metal-fullerene coordination complexes.

Acknowledgements

The work was supported by Russian Science Foundation (project N 14-13-00028) and Grant-in-Aid Scientific Research from JSPS, Japan (23225005 and 26288035). Y. N. is indebted to JGC-S SCHOLARSHIP FOUNDATION. Theoretical calculations were performed at the Research Center for Computational Science, Okazaki, Japan.

Notes and references

[a]Institute of Problems of Chemical Physics RAS, Chernogolovka, Moscow region, 142432 Russia;
[b]Institute of Solid State Physics RAS, Chernogolovka, Moscow region, 142432 Russia;
[c]Chemistry Department, Moscow State University, Leninskie Gory,119991 Moscow, Russia;
[d]Research Center for Low Temperature and Materials Sciences, Kyoto University, Sakyo-ku, Kyoto 606-8501, Japan;
[e]Faculty of Agriculture, Meijo University, 1-501 Shiogamaguchi, Tempaku-ku, Nagoya 468-8502, Japan.

Electronic Supplementary Information (ESI) available: IR spectra of complexes **1**-**4**, figures with packing of complexes **3** and **4**, EPR spectra of complex **3**, and details of calculations for complexes **1** and **3**. This material is available free of charge via Internet at …..

1 B. Gotschy, *Fullerene Sci. and Technol*., 1996, **4**, 677.
2 K. Tanigaki and K. Prassides, *J. Mater. Chem*., 1995, **5**, 1515.
3 K. Prassides, The Physics of fullerenes-based and fullerene-related materials, W. Andreoni (Ed.), Kluwer Academic Publishers, Netherlands, 2000, 175.
4 D. V. Konarev, S. S. Khasanov, A. Otsuka, M. Maesato, G. Saito and R. N. Lyubovskaya, *Angew. Chem. Int. Ed. Engl.*, 2010, **49**, 4829.
5 A. L. Balch and M. M. Olmstead, *Chem. Rev*., 1998, **98**, 2123.
6 P. J. Fagan, J. C. Calabrese and B. Malone, *Acc. Chem. Res.*, 1992, **25**, 134.
7 A. L. Balch, V. J. Catalano, J. W. Lee and M. M. Olmstead, *J. Am. Chem. Soc.*, 1992, **114**, 5455.
8 D.V. Konarev, S.S. Khasanov, S.I. Troyanov, Y. Nakano, K. A. Ustimenko, A. Otsuka, H. Yamochi, G. Saito and R. N. Lyubovskaya, *Inorg. Chem*., 2013, **52**, 13934.
9 I. J. Mavunkal, Y. Chi, S. -M. Peng and G. -H. Lee, *Organometallics*, 1995, **14**, 4454.
10 D. V. Konarev, S. S. Khasanov, E. I. Yudanova and R. N. Lyubovskaya, *Eur. J. Inorg. Chem.*, 2011, 816.
11 A. L. Balch, L. Hao and M. M. Olmstead, *Angew. Chem., Int. Ed. Engl.*, 1996, **35**, 188.
12 P. J. Fagan, J. C. Calabrese and B. Malone, *J. Am. Chem. Soc*., 1991, **113**, 9408.
13 D. V. Konarev, S. I. Troyanov, Y. Nakano, K. A. Ustimenko, A. Otsuka, H. Yamochi, G. Saito and R. N. Lyubovskaya, *Organometallics*, 2013, **32**, 4038.
14 D. V. Konarev, S. I. Troyanov, Y. Nakano, A. Otsuka, H. Yamochi, G. Saito and R. N. Lyubovskaya, *Dalton Trans*., 2014, **43**, 17920.
15 D. V. Konarev, S. S. Khasanov, Y. Nakano, A. Otsuka, H. Yamochi, G. Saito and R. N. Lyubovskaya, *Inorg. Chem.* 2014, **53**, 11960.
16 V. I. Sokolov, R. G. Gasanov, L. Y. Goh, Z. Weng, A. L. Chistyakov and I. V. Stankevich, *J. Organomet. Chem.* 2005, **690**, 2333.
17 R. G. Gasanov, A. S. Lobach, V. I. Sokolov1, A. P. Demenjev, K. I. Maslakov and E. D. Obraztsova, *J. Nanosci. Nanotechno.*, 2007, **7**, 1.
18 S. Zhang, T. L. Brown, Y. Du and J. R. Shapley, *J. Am. Chem. Soc*., 1993, **115**, 6705.
19 F. L. Bowles, M. M. Olmstead and A. L. Balch, *J. Am. Chem. Soc*., 2014, **136**, 3338.
20 M. N. Bengough, D. M. Thompson, M. C. Baird and G. D. Enright, *Organometallics* 1999, **18**, 2950.
21 D. M. Thompson, J. H. Brownie and M. C. Baird, *Fuller. Nanotub. Car. Nanostr.* 2004, **12**, 697.
22 D. M. Thompson, M. N. Bengough and M. C. Baird, *Organometallics* 2002, **21**, 4762.
23 D. M. Thompson, M. Jones and M. C. Baird, *Eur. J. Inorg. Chem.* 2003, 175.
24 D. V. Konarev, S. I. Troyanov, A. V. Kuzmin, Y. Nakano, S. S. Khasanov, A. Otsuka, H. Yamochi, G. Saito and R. N. Lyubovskaya, *Organometallics*, 2015, **34**, 879.
25 R. D. Adams, D. M. Collins and F. A. Cotton, *Inorg. Chem*., 1974,

13, 1086.
26 R. O. Loutfyc, C. K. Hsiao, B. S. Ong and B. Keoshkerian, *Can. J . Chem*. 1984, **62,** 1877.
27 D.V. Konarev and R.N. Lyubovskaya, *Russ. Chem. Rev*. 2012, **81**, 336.
28 C. A. Reed and R. D. Bolskar, *Chem. Rev*. 2000, **100**, 1075.
29 S. Chaiwasie and R. H. Fenn, *Acta Cryst. B*, 1968, **24**, 525.
30 J. -S. Huang and L. F. Dahl, *J. Organomet. Chem.*, 1983, **243**, 57.
31 X. Jin, X. Xie and K. Tang, *Chem. Commun.* 2002, 750.
32 K. Tang, S. Zheng, X. Jin, H. Zeng, Z. Gu, X. Zhou and Y. Tang, *J. Chem. Soc., Dalton Trans.* 1997, 3585.
33 H. -F. Hsu, Y. Du, T. E. Albrecht-Schmitt, S. R. Wilson and J. R. Shapley, *Organometallics*, 1998, **17**, 1756.
34 D. V. Konarev, S. S. Khasanov, A. Otsuka, Y. Yoshida, R. N. Lyubovskaya and G. Saito, *Chem. Eur. J*. 2003, **9**, 3837.
35 D. V. Konarev, S. S. Khasanov, A. Otsuka, G. Saito and R. N. Lyubovskaya, *Chem. Eur. J*. 2006, **12**, 5225.
36 D. V. Konarev, S. S. Khasanov and R. N. Lyubovskaya, *Russ. Chem. Bull*., 2007, **56**, 371.
37 D. V. Konarev, S. S. Khasanov and R. N. Lyubovskaya, *Coord. Chem. Rev*., 2014, **262**, 16.
38 K. B. Wiberg, *Tetrahedron*, 1968, **24**, 1083.
39 D. V. Konarev, N. A. Romanova, R. A. Panin, A. A. Goryunkov, S. I. Troyanov and R. N. Lyubovskaya, *Chem. Eur. J.*, 2014, **20**, 5380.
40 G. M. Sheldrick, *Acta Cryst. Sec. A*, 2008, **64**, 112.
41 Bruker AXS Inc., Madison, Wisconsin, USA.
42 a) T. Yanai, D. Tew and N. Handy, *Chem. Phys. Lett.*, 2004, **393**, 5; b) S. Grimme, J. Antony, S. Ehrlich and H. Krieg, *J. Chem. Phys.*, 2010, **132**, 154104.
43 R. Peverati and D. G. Truhlar, *J. Phys. Chem. Lett.*, 2011, **2**, 2810.
44 K. A. Peterson, D. Figgen, M. Dolg and H. Stoll, *J. Chem. Phys.*, 2007, **126**, 124101.
45 T. H. Dunning, Jr., *J. Chem. Phys.*, 1989, **90**, 1007.
46 NBO Version 3.1, E. D. Glendening, A. E. Reed, J. E. Carpenter and F. Weinhold.
47 Gaussian 09, Revision D.01, M. J. Frisch, G. W. Trucks, H. B. Schlegel, G. E. Scuseria, M. A. Robb, J. R. Cheeseman, G. Scalmani, V. Barone, B. Mennucci, G. A. Petersson, H. Nakatsuji, M. Caricato, X. Li, H. P. Hratchian, A. F. Izmaylov, J. Bloino, G. Zheng, J. L. Sonnenberg, M. Hada, M. Ehara, K. Toyota, R. Fukuda, J. Hasegawa, M. Ishida, T. Nakajima, Y. Honda, O. Kitao, H. Nakai, T. Vreven, J. A. Montgomery, Jr., J. E. Peralta, F. Ogliaro, M. Bearpark, J. J. Heyd, E. Brothers, K. N. Kudin, V. N. Staroverov, R. Kobayashi, J. Normand, K. Raghavachari, A. Rendell, J. C. Burant, S. S. Iyengar, J. Tomasi, M. Cossi, N. Rega, J. M. Millam, M. Klene, J. E. Knox, J. B. Cross, V. Bakken, C. Adamo, J. Jaramillo, R. Gomperts, R. E. Stratmann, O. Yazyev, A. J. Austin, R. Cammi, C. Pomelli, J. W. Ochterski, R. L. Martin, K. Morokuma, V. G. Zakrzewski, G. A. Voth, P. Salvador, J. J. Dannenberg, S. Dapprich, A. D. Daniels, Ö. Farkas, J. B. Foresman, J. V. Ortiz, J. Cioslowski, and D. J. Fox, Gaussian, Inc., Wallingford CT, 2009.

For Table of Content use only.

SYNOPSIS

Crystalline anionic coordination complexes of η^2-coordinated fullerenes C_{60} and C_{70} with cyclopentadienyl (**1**, **2**) and pentamethylcyclopentadienyl (**3**) molybdenum dicarbonyl have been obtained. The $\{CpMo^0(CO)_2(\eta^2\text{-}C_{60(70)})\}^-$ anions contain neutral C_{60} and C_{70} in **1** and **2,** whereas the $\{Cp^*Mo^I(CO)_2(\eta^2\text{-}C_{60}^-)\}^-$ anions contains more negatively charged fullerenes in **3**. Optical and magnetic properties as well as the DFT calculations for the complexes **1**-**3** are presented.

GRAPHIC

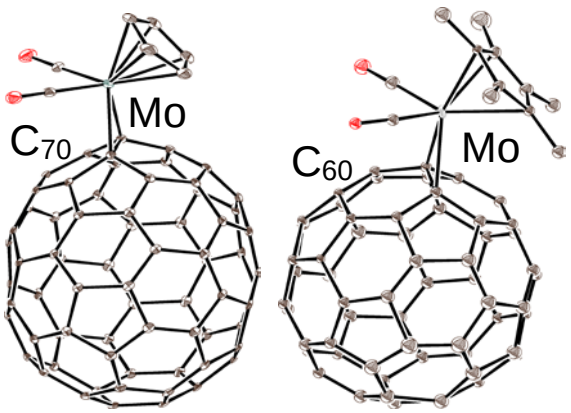

Crystalline molybdenum η^2-complexes with fullerenes C_{60} and C_{70} in neutral and negatively charged form were obtained and studied.